Molecular Biology of the Cell
Vol. 19, 3334–3346, August 2008

Sequential Actions of Myotubularin Lipid Phosphatases Regulate Endosomal PI(3)P and Growth Factor Receptor Trafficking

Canhong Cao,* Jonathan M. Backer,† Jocelyn Laporte,‡ Edward J. Bedrick,§ and Angela Wandinger-Ness*

*Department of Pathology, University of New Mexico School of Medicine and §Department of Mathematics and Statistics and Department of Internal Medicine, Albuquerque, NM 87131; †Department of Molecular Pharmacology, Albert Einstein College of Medicine, Bronx, NY 10461; and ‡Department of Molecular Pathology, Institut de Génétique et de Biologie Moléculaire et Cellulaire (IGBMC), INSERM U596, Centre National de la Recherche Scientifique UMR7104, Collège de France, University Louis Pasteur de Strasbourg, 67404 Illkirch, France

Submitted April 9, 2008; Revised May 19, 2008; Accepted May 22, 2008
Monitoring Editor: Sandra Schmid

Two different human diseases, X-linked myotubular myopathy and Charcot-Marie-Tooth disease, result from mutant MTM1 or MTMR2 lipid phosphatases. Although events involved in endosomal PI(3)P and PI(3,5)P_2 synthesis are well established and pivotal in receptor signaling and degradation, enzymes involved in phosphoinositide degradation and their roles in trafficking are incompletely characterized. Here, we dissect the functions of the MTM1 and MTMR2 myotubularins and establish how they contribute to endosomal PI(3)P homeostasis. By mimicking loss of function in disease through siRNA-mediated depletion of the myotubularins, excess PI(3)P accumulates on early (MTM1) and late (MTMR2) endosomes. Surprisingly, the increased PI(3)P blocks the egress of epidermal growth factor receptors from early or late endosomes, suggesting that the accumulation of signaling receptors in distinct endosomes may contribute to the unique disease etiologies when MTM1 or MTMR2 are mutant. We further demonstrate that direct myotubularin binding to the type III PI 3-kinase complex hVps34/hVps15 leads to phosphatase inactivation. The lipid kinase-phosphatase interaction also precludes interaction of the PI 3-kinase with Rab GTPase activators. Thus, unique molecular complexes control kinase and phosphatase activation and locally regulate PI(3)P on discrete endosome populations, thereby providing a molecular rationale for related human myo- and neuropathies.

INTRODUCTION

How phophoinositide synthesis and degradation are coordinately regulated remains a key question in endocytic membrane trafficking. The importance of phosphoinositides in endocytic trafficking has been largely studied by inhibiting lipid kinases or overexpressing lipid phosphatases to reduce lipid levels (Futter *et al.,* 2001; Chaussade *et al.,* 2003; Lu *et al.,* 2003; Petiot *et al.,* 2003; Tsujita *et al.,* 2004; Johnson *et al.,* 2006). The fact that inactivation of lipid phosphatases results in disease points to the importance of optimal phosphoinositide levels in homeostasis (Laporte *et al.,* 1996; Bolino *et al.,* 2000; Bitoun *et al.,* 2005; Niemann *et al.,* 2006; Spinosa *et al.,* 2008).

Endocytic membrane trafficking is critically dependent on the local synthesis of phosphatidylinositol 3-phosphate (PI(3)P) and phosphatidylinositol 3,5-phosphate (PI(3,5)P_2) (Futter *et al.,* 2001; Chaussade *et al.,* 2003; Ikonomov *et al.,* 2003; Lu *et al.,* 2003; Petiot *et al.,* 2003; Stein *et al.,* 2003; Tsujita *et al.,* 2004; Johnson *et al.,* 2006; Shisheva, 2008). PI(3)P is generated on early endosomes as well as on late endosomes by the type III PI 3-kinase complex hVps34/hVps15 (Gillooly *et al.,* 2000; Simonsen *et al.,* 2001; Stein *et al.,* 2003). PI(3)P is responsible for the temporal recruitment of proteins required for endosome fusion and membrane invagination. Endosomal synthesis of PI(3)P is initiated with the activation of the Rab5 and Rab7 GTPases on early and late endosomes, respectively (Christoforidis *et al.,* 1999; Feng *et al.,* 2001; Murray *et al.,* 2002; Stein *et al.,* 2003, 2005). The activated GTPases bind and recruit the hVps34/hVps15 PI 3-kinase complex via the hVps15 adapter and thereby locally activate PI(3)P synthesis. The subsequent conversion of PI(3)P into PI(3,5)P_2 occurs on multivesicular late endosomes, owing to the activity of the phosphoinositide kinase PIKfyve, and

This article was published online ahead of print in *MBC in Press* (http://www.molbiolcell.org/cgi/doi/10.1091/mbc.E08–04–0367) on June 4, 2008.

Address correspondence to: Angela Wandinger-Ness (wness@unm.edu).

Abbreviations used: CMT, Charcot-Marie-Tooth; EEA1, early endosome antigen 1; EGFR, epidermal growth factor receptor; FYVE, Fab1p, YOTB, Vac1p and EEA1 domain; GAPDH, glyceraldehyde-3-phosphate dehydrogenase; GRAM, glucosyltransferases, Rablike GTPase activators and myotubularin domain; GroP, glycerophosphoinositol phosphates; HEAT, Huntington, EF-3, PR65/A and mTOR domain; Hrs, hepatocyte growth factor–regulated tyrosine kinase substrate; hVps, human vacuolar protein sorting; MTM1, myotubularin 1; MTMR2, myotubularin-related protein 2; MVB, multivesicular body; (PI(3)P), phosphatidylinositol 3-phosphate; (PI(3,5)P_2), phosphatidylinositol 3,5-phosphate; PKD, protein kinase domain; Tsg, tumor susceptibility gene; WD40, beta-propeller domain or beta-transducin repeats.

leads to protein sorting into intralumenal vesicles and control of lysosome size (Rudge *et al.*, 2004; Nicot *et al.*, 2006; Shisheva, 2008). Thus, the enzymes and pathways involved in endosomal phosphatidyl inositol phosphate synthesis are well established.

On the other hand, the identity of the lipid phosphatases responsible for the degradation of endosomal PI(3)P or PI(3,5)P_2 are still debated and poorly defined (Tsujita *et al.*, 2004; Lorenzo *et al.*, 2006). Although the enzymology and structure of myotubularins have been intensively investigated, their cellular functions and regulation remain enigmatic (Begley and Dixon, 2005). In vitro assays show the myotubularins MTM1 and MTMR2 utilize both PI(3)P and PI(3,5)P2 as substrates (Blondeau *et al.*, 2000; Taylor *et al.*, 2000; Berger *et al.*, 2002; Tronchere *et al.*, 2004). Our own work shows MTM1 is recruited to early endosomes and to some extent late endosomes (Cao *et al.*, 2007). Existing functional data show MTM1 overexpression depletes PI(3)P staining and early endosome antigen 1 (EEA1) membrane association, yet effects on EGF receptor (EGFR) degradation suggested a late function, thus there exists a lack of clarity as to the specific endosomal function of MTM1 (Kim *et al.*, 2002; Chaussade *et al.*, 2003; Tsujita *et al.*, 2004). MTMR2 overexpression reduced cellular PI(3)P pools by 'mass action' based on biotinylated-GST-2xFYVE^{Hrs} staining (Lorenzo *et al.*, 2006); however, MTMR2 functions in endocytic trafficking were not elucidated. Furthermore, suggested mass action effects contradict other studies and cannot explain the unique disease etiologies that result when MTM1 or MTMR2 are mutated (Laporte *et al.*, 1996; Berger *et al.*, 2002; Kim *et al.*, 2002; Laporte *et al.*, 2002). Loss of myotubularin (MTM1) and myotubularin-related protein (MTMR2) functions are linked to muscle wasting or peripheral nerve dysfunction in humans, respectively, suggesting the proteins may have nonoverlapping functions (Laporte *et al.*, 2002). Overall, the myotubularins MTM1 and MTMR2 appear ideally poised to regulate the degradation of endosomal PI(3)P and PI(3,5)P_2 pools, yet their specific cellular functions remain of interest. In addition, the mechanisms whereby myotubularins interface with enzymes involved in phosphoinositide synthesis and contribute to the control of homeostasis are important open questions.

Here, we mimic loss of lipid phosphatase functions associated with human diseases by siRNA-mediated depletion of MTM1 or MTMR2 and assess individual myotubularin functions in endocytic trafficking. The mechanisms controlling myotubularin activity are investigated to gain new insight into the regulation of phosphoinositide homeostasis.

MATERIALS AND METHODS

Cell Culture and Transfection, Reagents and Antibodies, Plasmids and siRNA Construction, and Quantitative Real-Time PCR

Descriptions are provided in the online Supplementary Material. All reagents were purchased from Sigma-Aldrich (St. Louis, MO) unless otherwise specified.

EGFR Internalization and Degradation Assays

Cell surface EGFR and initial internalization rates were measured by flow cytometry (online Supplementary Material). For degradation assays, A431 cells or SCC-12F cells grown in six-well plates were serum starved for 2 h in DMEM with 25 μg/ml cycloheximide and stimulated with 100 ng/ml (A431 cells) or 20 nM (SCC-12F cells) epidermal growth factor (EGF; Invitrogen, Carlsbad, CA) and 25 μg/ml cycloheximide. At time points (0–4 h), cells were lysed with 80 μl SDS lysis buffer (10 mM Tris, pH 7.5, 140 mM NaCl, 1% [wt/vol] SDS, 5 mM EDTA, 2 mM EGTA, 1 mM PMSF, and protease inhibitor cocktail CLAP: 10 μg/ml chymostatin, leupeptin, antipain, and pepstatin A, 1 mM Na_3VO_4) and brief sonication to shear DNA. Cellular debris was removed by centrifugation, and total protein concentration was quantified using Bio-Rad DC protein assay (Richmond, CA). Assays were repeated at least three times in each of the two cell lines and analyzed as detailed in *Statistical Analyses*.

Immunofluorescence Microscopy

Cells grown on coverslips were processed for immunofluorescence staining as described (Stein *et al.*, 2005). Cells transfected with Cy3-labeled siRNA were permeabilized for 5 min with 0.01% saponin-PIPES, fixed with 3% paraformaldehyde, and permeabilized for 5 min in 0.1% (vol/vol) Triton. Blocking and antibody incubations included 0.4% fish skin gelatin. Coverslips were viewed on a Zeiss LSM 510 confocal microscope (Thornwood, NY) using plan-Neofluor 40×/1.30 oil or plan-Neofluor 63×/1.30 oil objectives, taking 0.5-μm optical sections at variable zooms. All images were exported as tiff files and compiled in Adobe Photoshop (San Jose, CA). For comparative analyses, cells were imaged under identical parameters, and fluorescence intensity analyzed using Slidebook 4.1 software (Intelligent Imaging Innovations, Denver, CO). The fluorescence intensity for cellular green fluorescent protein (GFP)-2xFYVE^{Hrs}, EEA1, and Rab7 staining is the average pixel intensity above the background threshold.

Coimmunoprecipitation and Western Blot

Cell lysates were prepared and immunoprecipitations were performed in RIPA buffer as previously described (Stein *et al.*, 2005). Proteins were resolved by SDS-PAGE on 8–12% gels and transferred to nitrocellulose membranes (Amersham Biosciences, Piscataway, NJ). Proteins were visualized with horseradish peroxidase–conjugated antibodies directed against rabbit or mouse Ig and Super Signal West Pico chemiluminescent substrate (Pierce Biotechnology, Rockford, IL). The chemiluminescent signal on the immunoblots were quantified with GS-800 Calibrated Densitometer and Quantity-One software (Bio-Rad).

Glutathione S-Transferase Pulldown

Recombinant MTMR2 was expressed as an N-terminal glutathione *S*-transferase (GST) fusion protein in *Escherichia coli* BL21 and purified, yielding 10 mg/400 ml culture (Stein *et al.*, 2005). Full-length (hVps15wt), hVps15 domain-deletion mutants or hVps15 domains were synthesized in vitro using TNT Quick Coupled Transcription/Translation system (Promega, Madison, WI). In vitro–translated products, 10 μl, were added individually to equimolar GST-MTMR2 or GST immobilized on glutathione-Sepharose beads and incubated at 4°C for 2 h. Precipitated proteins were solubilized in 2× SDS sample buffer, resolved by SDS-PAGE on 10% gels, and quantified by Phosphoimage Storm 860 (Molecular Dynamics, Sunnyvale, CA).

PI(3)P Phosphatase Activity

Phosphatase activity was detected as described with some modification (Taylor and Dixon, 2001). Coimmunoprecipitated or GST pulldown protein complexes on beads were prepared as above. Phosphatase activity was measured in 30 μl 50 mM ammonium acetate, pH 6.0, and 2 mM DTT containing 1.5 μg NBD6-PI(3)P as the substrate (Echelon Research Labs, Salt Lake City, UT) for 15 min at 30°C. In some samples, 100 nM wortmannin was added 15 min before substrate addition (Wymann *et al.*, 1996). Beads were removed by centrifugation, and 100 μl acetone wash was combined with the assay supernatant. Samples were dried under nitrogen. The dried reaction products were spotted onto glass-backed silica gel 60 plates (Whatman International, Kent, United Kingdom) in methanol/2-propanol/glacial acetic acid (5/5/2) and developed in chloroform/methanol/acetone/glacial acetic acid/water (70/50/20/20/20). Silica gel plates were pretreated as described (Walsh *et al.*, 1991). Fluorescent lipids were visualized and quantified using a NucleoTech UV system (Palo Alto, CA).

Metabolic Labeling of Cells with myo-[2-^{3}H]Inositol and HPLC Separation of Glycerophosphoinositol Phosphates

At 24 h after siRNA duplex transfection, A431 cells in 60-mm dishes were starved in inositol-free DMEM containing 1 mg/ml fatty acid free bovine serum albumin for 6 h. Cells were metabolically labeled with 25 μCi/ml myo-[2-^{3}H]inositol (Amersham Biosciences) for 36 h and stimulated with 100 ng/ml EGF for 10 min (Dadabay *et al.*, 1991; Sbrissa and Shisheva, 2005). Cultures were washed once with cold Tris-buffered saline (TBS). One milliliter, ice-cold 2.4 M HCl was added, and samples were transferred to a polypropylene tube. Lipids were extracted with 2.5 ml chloroform:methanol (3:2) with 10 μg phosphoinositides as carrier. After brief, low-speed centrifugation at 4°C, the bottom phase was transferred to a new polypropylene tube. The top phase was re-extracted once with 1 ml chloroform. The extracted lipids were dried under nitrogen, deacylated by incubation with 200 μl 33% methylamine at 50°C for 1 h, dried again, and resuspended in water. After two extractions with *n*-butanol:petroleum ether:ethyl formate (20:4:1), water-soluble glycerophosphoinositol phosphates (GroP) were dried, resuspended in water, and analyzed by anion-exchange HPLC on a Whatman Partisil SAX-5 column (Florham Park, NJ). ^{3}H-labeled PI(3)P, PI(4)P, PI(3,5)P_2, and PI(4,5)P_2 standards from yeast were prepared as described and were

generously provided by Dr. L. Weisman (University of Michigan; Stephens *et al.*, 1989; Backer *et al.*, 1993). Individual GroP species were eluted with a gradient based on buffers A (water) and B [1.25 M $(NH_4)_2HPO_4$, adjusted to pH 3.8 with H_3PO_4 at 25°C] at a flow rate of 1.0 ml/min; for 0 min, 0% in B; 5 min, 3% in B; 45 min, 12% in B; 52 min, 20% in B; and up to 100% in B over 50 min. Individual peak radioactivity was presented as a percentage of the summed radioactivity from all ^{3}H-labeled GroP species (total radioactivity).

PI(3)P Mass Strip Assay

Forty-eight hours after siRNA duplex transfection, A431 cells in 60-mm dishes were stimulated with 100 ng/ml EGF for 10 min. Extraction of PI(3)P from cells, detection, and quantification of PI(3)P were performed with an Echelon PI(3)P mass strip kit according to the manufacturer's instructions (custom prepared and now commercially available as K-2400 from Echelon Research Labs). The strips have prespotted PI(3)P standards and an array of phosphoinositides that serve as specificity controls. The PI(3)P in cell lysates were immunoisolated by beads bearing a specific anti-PI(3)P antibody that are supplied in the kit, and PI(3)P was released in solvent and spotted on the blank areas of the strip. A template of the mass strip layout is shown in Figure 1B. The strips are then probed with anti-PI(3)P antibody to visualize the PI(3)P standards and samples. Densitometry was used to quantify the PI(3)P standards. Sample values falling within the linear range of standards run on the same strip and exposed for the identical time are reported.

Statistical Analyses

Data shown in this manuscript are representative of multiple independent trials with the n values given in the legend. Graphs include bars that represent the SEM. Student's *t* test was used to calculate p values and identify statistically significant differences among pairs of data sets. Individual p values are included in each figure legend. Multiple statistical tools (Student's *t* test, repeated measures analysis, one-way ANOVA, and Tukey method) were used to evaluate the observed changes in EGFR degradation kinetics (details in online Supplementary Materials).

RESULTS

Regulation of Endosomal PI(3)P through Differential Localization and Function of Myotubularins

MTM1 and MTMR2 overexpression decrease cellular PI(3)P based on GST-2xFYVE^{Hrs} staining (Kim *et al.*, 2002; Lorenzo *et al.*, 2006). Endosomal PI(3)P is synthesized by the hVps34/hVps15 kinase and serves in the membrane recruitment of FYVE-domain–containing proteins. Among the FYVE-domain proteins, the PIKfyve PI 3-phosphate 5-kinase both binds and utilizes PI(3)P as its substrate. The product of PIKfyve, PI(3,5)P_2, in turn also serves as an in vitro substrate for MTM1 and MTMR2 (Sbrissa *et al.*, 2002; Tronchere *et al.*, 2004; Ikonomov *et al.*, 2006). Given the close metabolic relationship between PI(3)P and PI(3,5)P_2, it was of interest to determine the effects of MTM1 and MTMR2 depletion on cellular and endosomal PI(3)P and PI(3,5)P_2 levels using biochemical and morphological approaches.

To ablate myotubularin expression, we designed several siRNAs specifically targeted to MTM1 or MTMR2 mRNAs (online Supplementary Figure S1). High siRNA transfection efficiencies (95%) decreased protein and mRNA levels up to ninefold. Only the two most effective siRNAs (MTM1 209 and MTMR2 19) were used further. Off-target effects were minimal based on the fact that siRNA depletion of each myotubularin was specific and did not affect the levels of the other highly homologous myotubularin. Additionally, mock, scrambled, or glyceraldehyde 3-phosphate dehydrogenase (GAPDH) siRNA-transfected controls were included in all experiments to ensure specificity.

Effects on total cellular PI(3)P levels were quantitatively measured by radiolabeling control and myotubularin-depleted cells with myo-[2-^{3}H]inositol and analyzing the isolated GroPs by HPLC. Myotubularin depletion did not change total cellular PI(4)P and PI(4,5)P_2 pools (Figure 1A) but did result in a 60–120% increase in total cellular PI(3)P pools (Figure 1A, $p < 0.01$–0.05). A 140–250% increase in PI(3)P levels was detected in MTM1- or MTMR2-depleted samples with a PI(3)P strip (Figure 1B, $p < 0.05$). The concurrence of quantitative changes in PI(3)P levels using two independent assays provides strong evidence for the importance of both MTM1 and MTMR2 activities in phosphoinositide homeostasis and establishes the PI(3)P mass strip assay as a useful method for assessing changes in cellular PI(3)P levels that may substitute for radiolabeling and HPLC.

PI(3,5)P_2 in human cells constitutes <1% of the total phosphatidylinositol lipid pool, making it difficult to detect (Sbrissa and Shisheva, 2005; Pettitt *et al.*, 2006). By HPLC, depletion of MTMR2 resulted in a subtle increase in PI(3,5)P_2, but no detectable change in MTM1-depleted samples (Supplementary Figure S2). Using an antibody directed against PI(3,5)P_2, myotubularin-depleted cells had detectably higher PI(3,5)P_2 levels ($p < 0.0001$; Supplementary Figure S2).

In vivo changes in specific endosomal PI(3)P pools were measured in myotubularin-depleted cells expressing a GFP-2xFYVE^{Hrs} fusion protein as a sensor and staining for specific endosomal markers. Membrane bound EEA1, which contains a FYVE-domain, served both as an early endosomal marker and as a second probe for PI(3)P on early endosomes. GFP-2xFYVE^{Hrs} colocalizing with Rab7 was used to quantify late endosomal PI(3)P. Early endosomal PI(3)P increased ~86% (fraction GFP-2xFYVE^{Hrs} and EEA1 colabel, $p < 0.01$), whereas late endosomal PI(3)P levels did not change (fraction GFP-2xFYVE^{Hrs} and Rab7 colabel, $p = 0.38$) in MTM1 siRNA-transfected cells relative to controls (Figure 1C and Supplementary Figure S3). In contrast, early endosomal PI(3)P remained unchanged ($p = 0.53$) and late endosomal PI(3)P levels increased 19% ($p < 0.02$) in MTMR2 siRNA-treated cells versus controls (Figure 1C and Supplementary Figure S3).

The changes in specific endosomal PI(3)P pools after siRNA-mediated depletion of individual myotubularins imply differential function and possibly localization. As we showed, MTM1 localizes to Rab5-positive early endosomes and partially to Rab7-positive late endosomes (Cao *et al.*, 2007). Others localized MTMR2 using an enhanced GFP-tagged variant revealed a predominant cytosolic staining pattern with higher staining intensity in the perinuclear region, but no specific membrane association was noted (Kim *et al.*, 2002; Laporte *et al.*, 2002). As shown here, neither wild-type MTMR2 nor a catalytically inactive mutant MTMR2D320A (MTMR2DA) exhibited any colocalization with Rab5 (wt) or dilated early endosomes bearing the constitutively active Rab5Q79L (Figure 2, top four rows and insets). Endogenous MTMR2 also did not colocalize with EEA1 (Supplementary Figure S4). Furthermore, MTMR2wt overexpression did not affect EEA1 membrane association. In contrast, significant colocalization of MTMR2wt with the late endosomal Rab7 (wt) marker was apparent (Figure 2, row five). The late endosomal localization of the catalytically inactive MTMR2D320A mutant was identical to the wild-type protein (Figure 2, row six). Endogenous MTMR2 was notably colocalized with Rab7-positive late endosomes, but also present on vesicles lacking late endosomal markers. (Supplementary Figure S4).

Together, the data show that MTM1 plays a pivotal role in regulating early endosomal PI(3)P levels, whereas MTMR2 is preferentially localized to late endosomes where it modulates late endosomal PI(3)P levels.

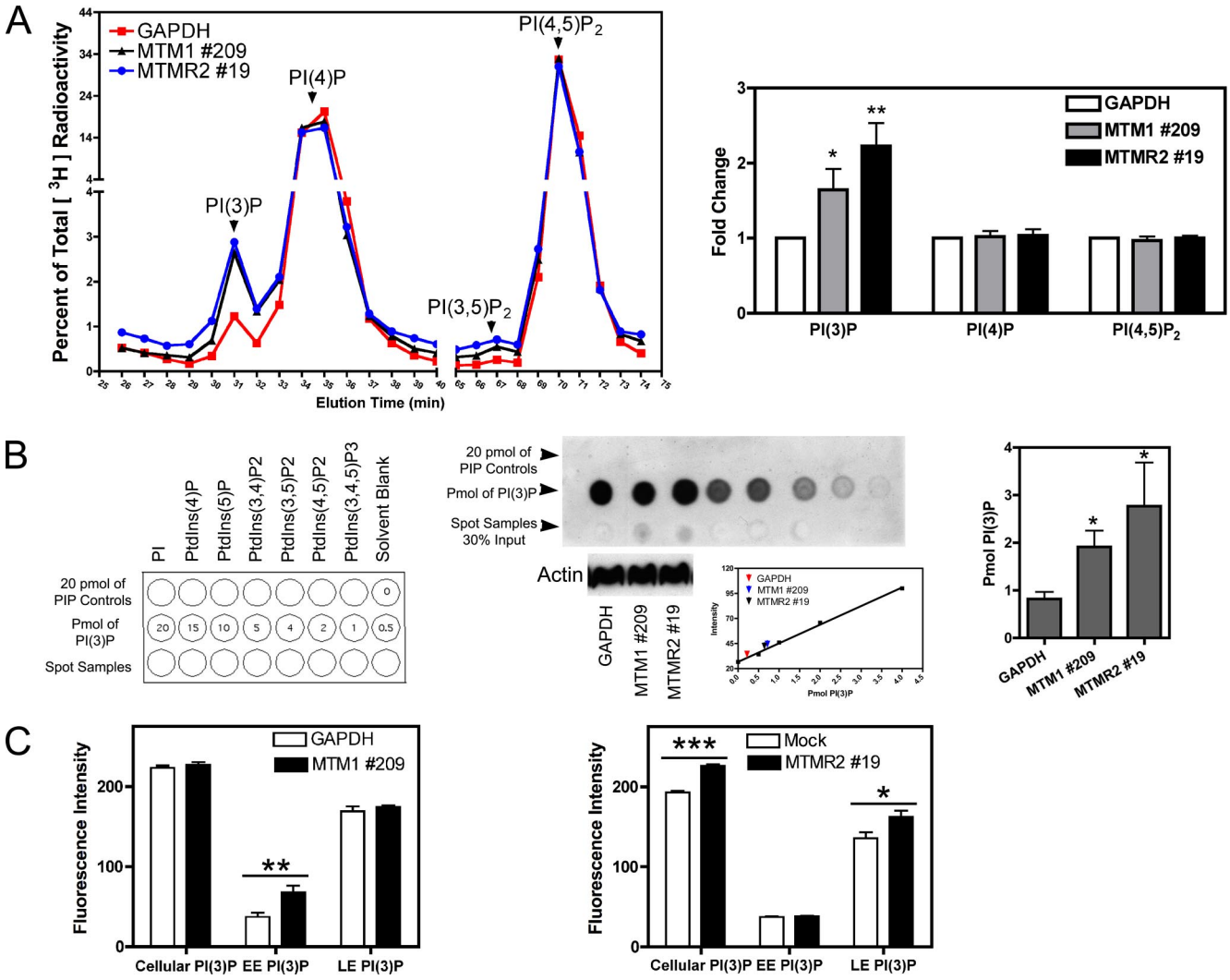

Figure 1. MTM1 or MTMR2 depletion increases cellular PI(3)P levels. A431 cells were transfected with MTM1 or MTMR2 siRNA. GAPDH siRNA-transfected samples served as negative controls. (A) Cells were metabolically labeled with myo-[2-^{3}H]inositol. Individual GroPs were resolved by HPLC. Chromatogram shows percentage of the summed radioactivity from all GroP species (total ^{3}H radioactivity) as a function of elution time for each indicated sample. Individual GroP species are quantified by area integration and normalized to controls (bar graph, mean ± SEM, n = 3–4, unpaired *t* test, two-tailed $^{**}p < 0.01$, $^{*}p < 0.05$). (B) PI(3)P were extracted and detected with an Echelon mass strip assay. Left panel, the PI(3)P strip template; middle panel, a representative PI(3)P strip with triangles highlighting controls, standards, or samples and an immunoblot for actin in each sample to confirm equal amounts of cells used for PI(3)P isolation. A standard curve shows the chemiluminescent signal intensity as a function of pmol of spotted PI(3)P standard. Right bar graph shows PI(3)P amounts in each sample (mean ± SEM, n = 3–4, unpaired *t* test: MTM1 209, two-tailed $^{*}p < 0.05$; MTMR2 19, one-tailed $^{*}p < 0.05$). (C) A431 cells were cotransfected with Cy3-labeled MTM1 or MTMR2 siRNA (red) and GFP-2xFYVE^{Hrs} (green). Cy3-labeled GAPDH siRNA (red) or mock-transfected samples served as controls. Endogenous EEA1 (blue) and Rab7 (blue) were detected with immunofluorescence staining. Samples were scanned at identical settings on confocal microscope. Fluorescence intensity of cellular PI(3)P levels (total membrane bound GFP-2xFYVE^{Hrs}), early endosomal (EE) PI(3)P levels (GFP-2xFYVE^{Hrs} colocalizing with EEA1) and late endosomal (LE) PI(3)P levels (GFP-2xFYVE^{Hrs} colocalizing with Rab7) in each sample is the average pixel intensity in the selected cell that is above the threshold quantified using Slidebook 4.1 image analysis software. Increase in EE PI(3)P of 86% (mean ± SEM, n = 10, unpaired *t* test, two-tailed $^{**}p < 0.01$) in MTM1 siRNA-transfected cells versus GAPDH control. Left panel, cellular PI(3)P and LE PI(3)P in MTM1 siRNA-transfected cells do not change relative to GAPDH control (mean ± SEM, n = 10, unpaired *t* test, two-tailed p = 0.36, 0.38) . Increase in cellular PI(3)P of 17% (mean ± SEM, n = 20, unpaired *t* test, two-tailed $^{***}p < 0.0001$) and in LE PI(3)P of 19% (mean ± SEM, n = 12, unpaired *t* test, two-tailed $^{*}p < 0.02$) in MTMR2 siRNA-transfected cells versus mock control. Right panel, EE PI(3)P levels remains unchanged in the presence of MTMR2 siRNA compared with mock control (mean ± SEM, n = 20, unpaired *t* test, two-tailed p = 0.53).

Endosomal Transport Depends on Sequential Myotubularin Function

On the basis of the distinct localizations and functions in PI(3)P regulation of the two myotubularins, we examined whether endocytosis is differentially regulated by monitoring EGFR internalization and degradation in two different epithelial cell lines. The human keratinocyte cell lines SCC-12F, expressing 2 × 10^5 EGFR per cell with well-described EGFR degradation kinetics, and A431 cells, expressing 10-fold higher levels of EGFR (Krupp *et al.*, 1982; Gamou *et al.*, 1984), were transfected with either MTM1 or MTMR2 siRNAs (Hudson *et al.*, 1986; McCawley *et al.*, 1997). Depletion of MTM1 or MTMR2 in SCC-12F cells slowed EGFR degradation to similar extents 15–30 min after ligand stimulation

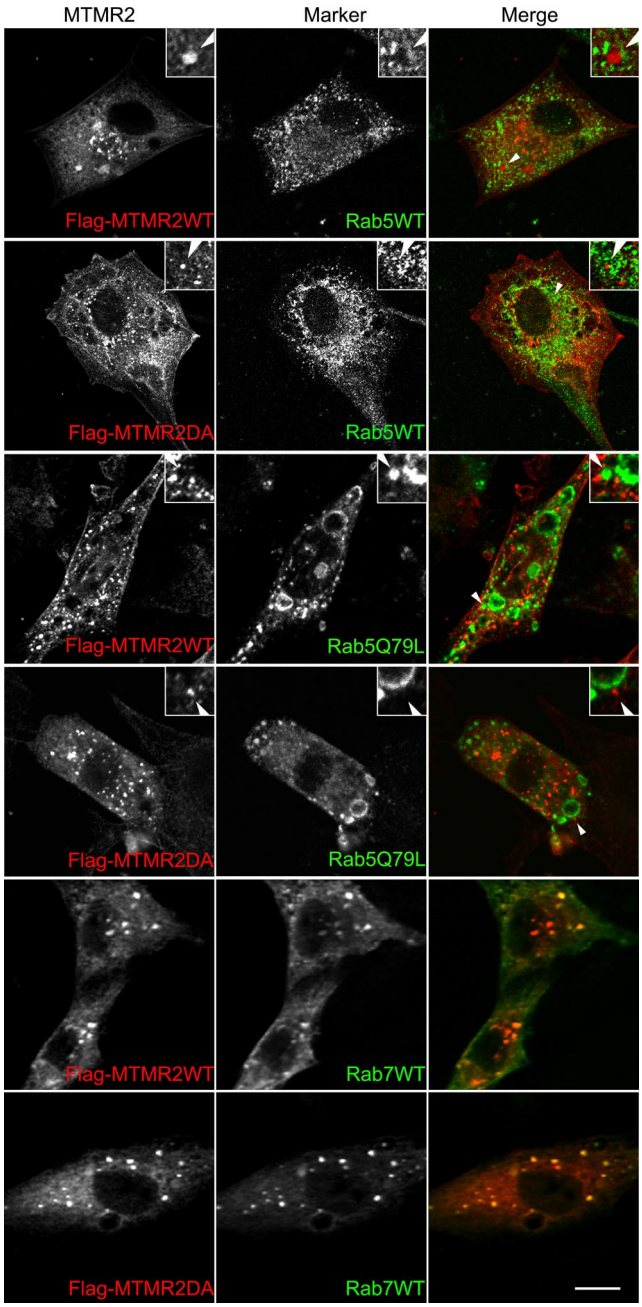

Figure 2. MTMR2 localizes to Rab7-positive late endosomes and is not detected on Rab5-positive early endosomes. BHK cells transiently transfected with Flag-MTMR2wt or Flag-MTMR2D320A (catalytically inactive mutant) were detected with immunofluorescence staining for Flag-MTMR2 (red) and the cotransfected endosomal markers, Rab5 (green) and Rab7 (green). Rab5Q79L (constitutively active mutant) facilitates analysis of recruitment to enlarged Rab5-positive early endosomes. Colocalization is yellow in color merge. Enlarged views of marked areas (insets) demonstrate the absence of any colocalization. Images were collected using 40× objective and scan zoom 3.0. Bar, 10 μm.

(Figure 3A). In A431 cells, where ligand-stimulated EGFR degradation occurs over a longer time, a notable kinetic distinction between MTM1 and MTMR2 depletion could be observed (Figure 4A). MTM1-depletion slowed EGFR degradation earlier and resulted in statistically significant higher EGFR levels beginning at 2 h, whereas MTMR2 effects did not appear before 3 h.

To distinguish if impaired EGFR degradation upon myotubularin depletion was due to decreased internalization rates or altered intracellular trafficking kinetics, immunofluorescence microscopy and quantitative flow cytometry were used. In the absence of stimulation, myotubularin-depleted SCC-12F cells looked identical to controls (Figure 3A) with EGFR predominantly cell surface localized (Figure 3, B and C). A431 cells exhibited a 60% (MTMR2) to 150% (MTM1) increase in basal EGFR levels, which was distributed between the cell surface and intracellular locations (Figure 4, A and B). In both cell lines, EGFR internalization in response to ligand stimulation was unaffected by myotubularin depletion (Figures 3, B and C, and 4C).

Immunofluorescence staining was used to evaluate if EGFR accumulated in specific endosomal compartments after MTM1 or MTMR2 depletion. At 15 min after stimulation, EGFR was exclusively intracellular in all SCC-12F samples and only partially in early endosomes, making it difficult to distinguish if EGFR accumulated in discrete endosomal compartments after myotubularin depletion (Figure 3B). However, in A431 cells, the delay in EGFR degradation was readily apparent upon depletion of either myotubularin, in agreement with immunoblot data (Figure 5, A–C, and Supplementary Figure S5). After 3 h of EGF stimulation, EGFR could only be detected in occasional cells of control samples. In ligand-stimulated, MTM1-depleted cells, EGFR accumulated intracellularly, where it was detected in EEA1 marked early endosomes, but largely absent from Rab7-positive late endosomes. In contrast, EGFR predominated in Rab7-positive late endosomes, with a subfraction remaining in early endosomes of MTMR2-depleted cells. The accumulation of EGFR in distinct endosomes upon EGF stimulation concurs with the observed alterations in EGFR degradation kinetics and sites of PI(3) accumulation after siRNA-mediated silencing of MTM1 and MTMR2.

Exclusive Binding of MTMR2 or Rab7 to the PI 3-kinase Adapter, hVps15

PI(3)P formation on endosomes is regulated by the Rab5 and Rab7 small GTPases in concert with the hVps34/hVps15 PI 3-kinase complex. As shown here, myotubularin lipid phosphatases contribute to the degradation of endosomal PI(3)P levels, raising the question as to how biosynthetic and degradative pathways might be coupled to preclude futile cycling.

Recently, we identified a direct interaction between MTM1 and the PI 3-kinase adaptor hVps15 (Cao *et al.*, 2007). Here, we show that wild type and the catalytically inactive MTMR2 mutant colocalize with hVps34 and to a significant extent with Rab7, indicating a possible interrelationship between the three proteins (Figure 6A). Protein–protein interactions were tested by coimmunoprecipitation and showed MTMR2 coprecipitated with hVps34/hVps15 under conditions where the proteins were overexpressed (Figure 6B). Endogenous MTMR2 was also found complexed to hVps34 via coprecipitation experiments (not shown) as demonstrated for MTM1 (Cao *et al.*, 2007). Thus, both phosphatases associate with the hVps34/hVps15 PI 3-kinase complex in mammalian cells.

Rab7 binds to the hVps34/hVps15 PI 3-kinase complex via hVps15 (Stein *et al.*, 2003, 2005). To test if binding of Rab7 or MTMR2 to the hVps34/hVps15 complex is mutually exclusive as is the case for MTM1 (Cao *et al.*, 2007), further coimmunoprecipitation experiments were performed (Figure 6C, left panels). Immunoprecipitation using an anti-Rab7

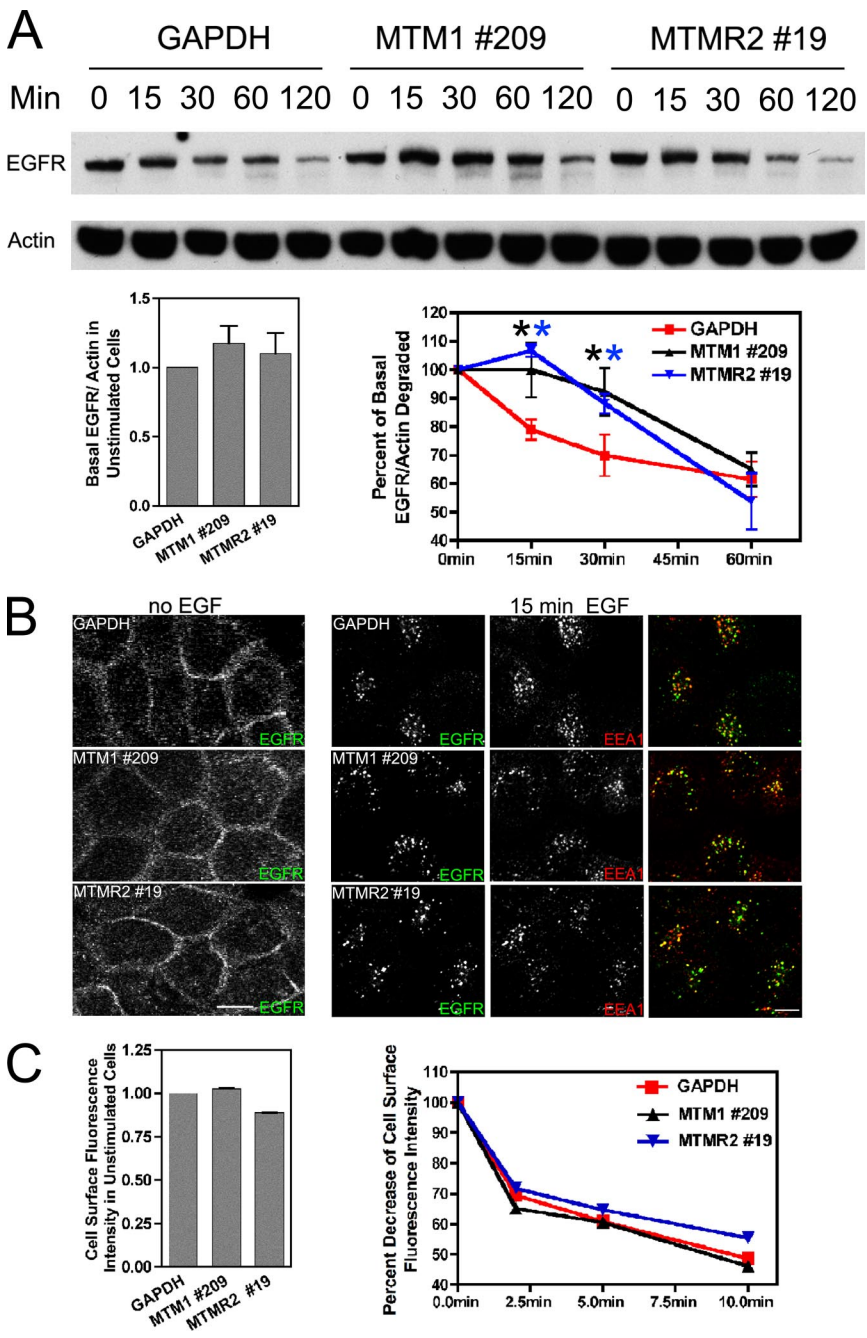

Figure 3. EGFR degradation after ligand stimulation is impaired in SCC-12F cells with myotubularin depletion. SCC-12F cells were transfected with MTM1 or MTMR2 siRNA. GAPDH siRNA-transfected samples served as negative controls. At 48 h after transfection, cells were stimulated with EGF for indicated time. (A) Total protein (10 μg/lane) was resolved by SDS-PAGE. Western blot shows EGFR and actin in each sample (top panel). The ratio of EGFR to actin was quantified with chemiluminescent signal on immunoblots by densitometry. Bar graph shows basal EGFR/actin in unstimulated cells normalized to negative control (mean ± SEM, n = 4, unpaired *t* test, two-tailed $p > 0.05$). Line graph shows percent of basal EGFR/actin degraded as a function of time after ligand stimulation (mean ± SEM, n = 4, unpaired *t* test, one-tailed $^*p < 0.05$). The details of additional statistical evaluations are given in Supplementary Methods. (B) Immunofluorescence staining shows EGFR localization (green) and EEA1 (red) in the indicated siRNA-transfected samples without ligand stimulation (no EGF) or with EGF stimulation for 15 min. Images were collected using 40× objective and scan zoom 1.8. Bar, 10 μm. (C) SCC-12F cells were transfected with Cy3-labeled MTM1 or MTMR2 siRNA. Cy3-labeled GAPDH siRNA-transfected samples served as negative controls. Cells were serum starved for 2 h and left unstimulated or stimulated with EGF up to 10 min. Cell surface EGFR was labeled with an anti-EGFR antibody conjugated to fluorescein and 20,000 cells were quantified by flow cytometry. Bar graph shows cell surface fluorescence intensity in unstimulated cells normalized to negative control and line graph shows percent decrease of cell surface fluorescence intensity as a function of time up to 10-min EGF treatment (mean ± SEM, n = 2).

antibody demonstrated that Rab7 and hVps15 were in a complex that did not include MTMR2. Conversely, immunoprecipitation of MTMR2 with an anti-FLAG antibody demonstrated that Rab7 was not present when MTMR2 was complexed to hVps15. We conclude, the hVps34/hVps15 complex binds to both Rab7 and MTMR2 but not simultaneously. A competitive in vitro binding experiment further substantiated the exclusive nature of the binding (Figure 6C, right panel). GST-MTMR2 was immobilized on glutathione-Sepharose beads and bound to saturating amounts of hVps15. Addition of increasing concentrations of Rab7-containing cell lysates (0, 1×, and10×) resulted in release of hVps15 from the GST-MTMR2 beads and into the supernatant fraction.

hVps15-MTMR2 Binding Is Mediated by Specific Domains

Domain mapping and in vitro binding studies were conducted to characterize the interactions between MTMR2 and hVps15 (Figure 6, D–G). WD40 and HEAT deletion mutants were coprecipitated with MTMR2 at 0.6- and 0.4-fold lower levels, respectively, than hVps15wt (Figure 6D), indicating their importance for MTMR2 binding. All hVps15 deletion constructs are properly folded and retain their ability to bind to hVps34 (Cao *et al.*, 2007). Conversely, mapping of the MTMR2 domains responsible for binding to hVps15 revealed that both the PH- and PTP-domains of MTMR2 were important, but the coiled-coil-domain was dispensable (Figure 6, F and G). In vitro GST pulldown experiments verified the direct interaction between hVps15 and MTMR2 (Figure

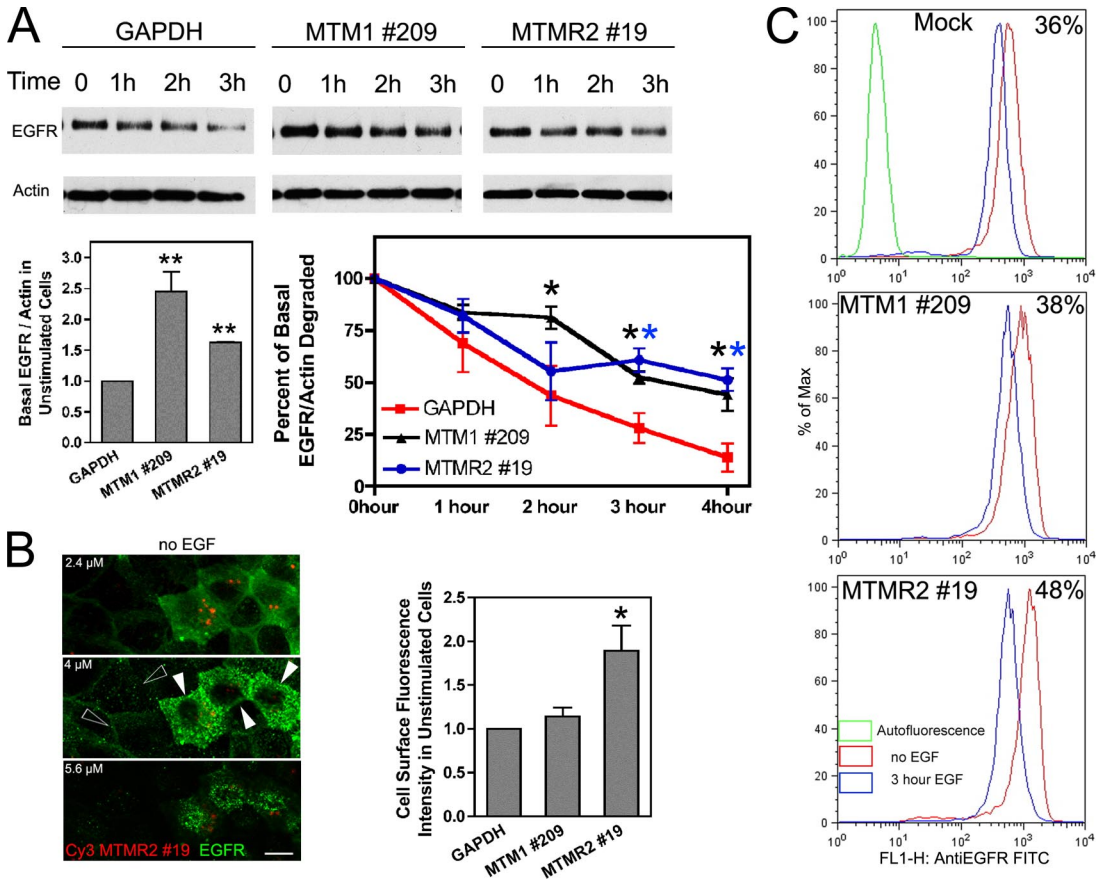

Figure 4. EGFR degradation after ligand stimulation is impaired in A431 cells with myotubularin depletion. (A) A431 cells were transfected with MTM1 or MTMR2 siRNA. GAPDH siRNA-transfected samples served as negative controls. At 48 h after transfection, cells were stimulated with EGF for indicated time. Total protein (2.5 μg/lane) was resolved by SDS-PAGE. Western blot shows EGFR and actin in each sample (top panel). The ratio of EGFR to actin was quantified with chemiluminescent signal on immunoblots by densitometry. Bar graph shows basal EGFR/actin in unstimulated cells normalized to negative control (mean ± SEM, n = 3, unpaired *t* test, two-tailed **$p < 0.01$). Line graph shows percent of basal EGFR/actin degraded as a function of time after ligand stimulation (mean ± SEM, n = 3–8, unpaired *t* test, MTM1 209: 2 h one-tailed *$p < 0.05$; 3 h two-tailed *$p < 0.05$; 4 h two-tailed *$p < 0.05$; MTMR2 19: 3 h two-tailed *$p < 0.01$; 4 h two-tailed *$p < 0.01$). The details of additional statistical evaluations are given in Supplementary Methods. (B) A431 cells were transfected with Cy3-labeled MTMR2 siRNA (red) for 48 h. The micrograph shows EGFR localization (green) in MTMR2 siRNA-transfected (filled arrows) versus untransfected cells (open arrows). Images were collected using 40× objective and scan zoom 1.8. Bar, 10 μm. A431 cells were transfected with Cy3-labeled MTM1 or MTMR2 siRNA. Cy3-labeled GAPDH siRNA-transfected samples served as negative controls. At 48 h after transfection, cell surface EGFR was labeled with an anti-EGFR antibody conjugated to fluorescein, and 20,000 cells were quantified by flow cytometry for each sample. Bar graph shows cell surface fluorescence intensity normalized to negative control (mean ± SEM, n = 3, unpaired *t* test, two-tailed *$p < 0.05$). (C) A431 cells were transfected with Cy3-labeled MTM1 or MTMR2 siRNA. Mock-transfected samples served as negative controls. Cells were serum starved overnight and left unstimulated or stimulated with EGF for 3 h. Cell surface EGFR was labeled with an anti-EGFR antibody conjugated to fluorescein, and 20,000 cells were quantified by flow cytometry. Plotted are percentages of total cells analyzed (% of max) as a function of cell surface fluorescence intensity for indicated samples. The numbers inside each graph denote the percent decrease in cell surface fluorescence after 3 h EGF treatment compared with no EGF treatment.

6E and Supplementary Figure S6). Binding of individual in vitro–transcribed and –translated, ^{35}S-radiolabeled hVps15 proteins to equimolar amounts of control GST or GST-MTMR2 immobilized on glutathione-Sepharose was analyzed. Deletion of the WD40-domain of hVps15 reduced MTMR2 binding to background levels. Conversely, the WD40-domain expressed alone was able to bind to MTMR2, though at reduced levels relative to full-length hVps15. Deletion of either the HEAT- or the PKD-domain of hVps15 impaired binding to MTMR2, though there was no statistical difference compared with binding of full-length hVps15. The HEAT/WD40-domain rescued binding to a greater extent than the WD40 domain alone suggesting that both the HEAT- and the WD40-domains of hVps15 facilitate binding to MTMR2. Altogether, the results verify the direct interaction of hVps15 and MTMR2 and suggest that Rab7 and MTMR2 have overlapping binding sites on hVps15, thereby, explaining the mutually exclusive complexes observed in vivo between the PI 3-kinase and MTMR2 or Rab7.

hVps15-MTMR2 Binding Inhibits PI(3)P Phosphatase Activity

The observed binding between the MTMR2 phosphatase and hVps15 raises the question of functional significance. To test if hVps15 binding had any impact on MTMR2 PI(3)P phosphatase activity, hVps15 was immunoprecipitated, co-precipitated MTMR2 was detected by immunoblot, and MTMR2 PI(3)P phosphatase activity monitored with an in vitro assay (Figure 7A). Fluorescent PI(3)P substrate and PI

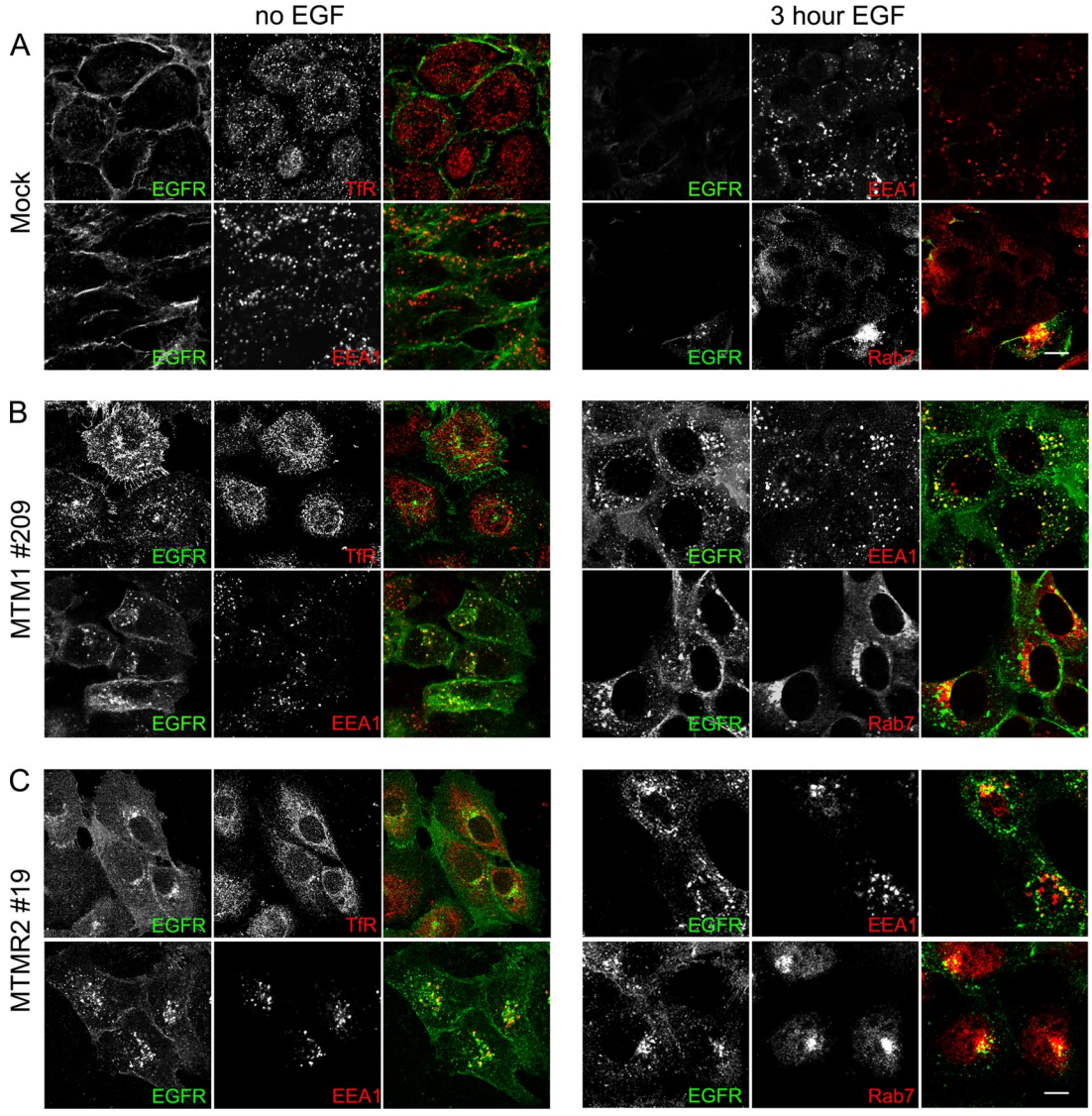

Figure 5. MTM1 and MTMR2 function differentially in endosomal sorting of EGFR. A431 cells were transfected with MTM1 or MTMR2 siRNA. Mock-transfected samples served as negative controls. At 48 h after transfection, cells were prepared for immunofluorescence staining without ligand stimulation (no EGF) or with EGF stimulation for 3 h. EGFR (green) was costained with transferrin receptor (TfR, red), EEA1 (red), or Rab7 (red) in indicated samples. (A) Mock-transfected cells, (B) MTM1 siRNA-transfected cells, (C) MTMR2 siRNA-transfected cells. Images were collected using 40× objective and scan zooms (A) 3.5, (B and C) 1.0. Bars, 10 μm.

product were resolved by TLC. Wild-type MTMR2 coprecipitated with an antibody against V5-hVps15 failed to degrade PI(3)P to PI, similar to the catalytically inactive mutant (DA) used as a control (Figure 7A, right two lanes). However, if the immunoprecipitation was performed using the same lysates except with an antibody against Flag-MTMR2, then the phosphatase activity was readily detected. Control immunoblots showed similar amounts of the MTMR2 phosphatase were precipitated with either antibody but the amount of interacting hVps15 was vastly different, thereby demonstrating that the overexpressed wild-type MTMR2 is active and incompletely complexed to hVps15 in vivo (Figure 7A). In vitro binding was used to demonstrate the dose-dependent inhibitory effect of hVps15 binding on MTMR2 phosphatase activity (Figure 7, B and C). The minimum amount of GST-MTMR2 required to convert 1.5 μg NBD6-PI(3)P into PI within 15 min in the phosphatase assay was established to be 60 ng GST-MTMR2, an amount used in all subsequent experiments (Figure 7B). A constant amount of GST-MTMR2 was immobilized on glutathione-Sepharose beads and incubated with increasing concentrations of hVps15-containing cell lysates. As hVps15 binding increased, MTMR2 PI(3)P phosphatase activity was increasingly inhibited (Figure 7C). A hVps15 WD40Δ-containing lysate exhibited reduced phosphatase inhibitory effect (Supplementary Figure S7). We were restricted to using mammalian cell lysates overexpressing hVps15 because bacterially expressed hVps15 is insoluble even when cells are cultured at low temperature to enhance proper folding. Endogenous hVps34 was below detectable levels and the only source of ATP required for kinase activity in the assay derived from the lysate, making it unlikely that endogenous hVps34 could mask the degradative activity of the MTMR2 in the phosphatase assay. To further exclude any contribution of PI 3-kinase activity, we coexpressed hVps15 with hVps34 and repeated the experiment. The presence of the

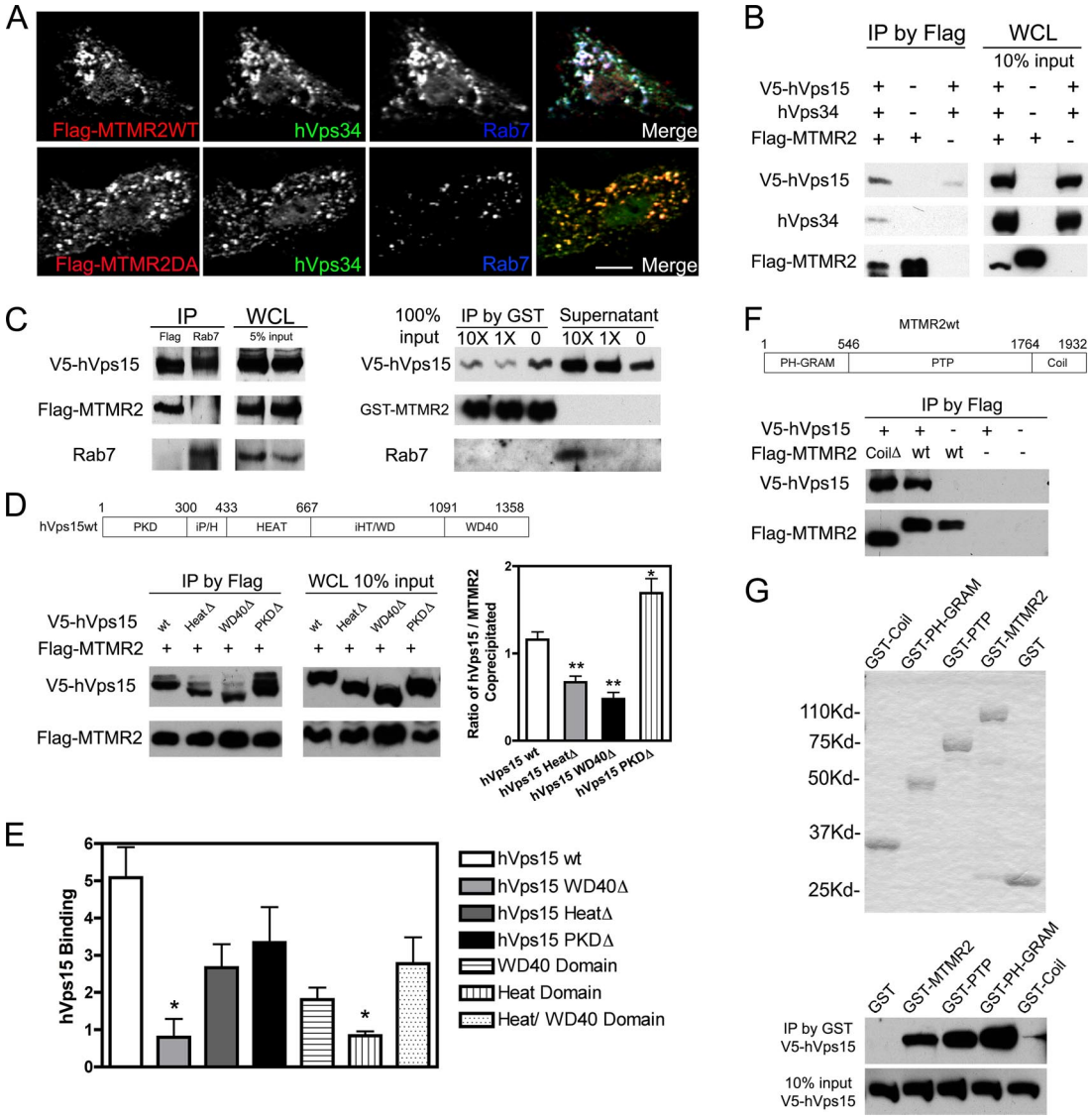

Figure 6. The WD40 domain of hVps15 mediates exclusive binding of MTMR2 or Rab7 to the hVps34/hVps15 PI 3-kinase complex. (A) BHK cells overexpressing Flag-MTMR2wt or Flag-MTMR2D320A (catalytically inactive mutant), hVps34 and Rab7 were immunostained. Images of Flag-MTMR2 (red), hVps34 (green), and Rab7 (blue) are shown in gray-scale and color merge. Color merge shows colocalization (white) of MTMR2 with hVps34 on Rab7-positive late endosomes. Images were collected using 40× objective and scan zoom 1.0. Bar, 10 μm. (B) BHK cells overexpressing Flag-MTMR2, hVps34 and V5-hVps15 were processed for immunoprecipitation (IP) with an anti-Flag mAb. Western blot shows coprecipitated hVps34 or hVps15 (left panel) and expression levels of individual protein in whole cell lysates (WCL) for each sample with indicated input amounts (right panel). MTMR2 associates with the hVps34/hVps15 complex. (C) BHK cells overexpressing Rab7, Flag-MTMR2 and V5-hVps15 were processed for IP with anti-Rab7 or anti-Flag antibodies, respectively. Western blot shows coprecipitated hVps15 (left panel) and WCL (middle panel). MTMR2 and Rab7 form a mutually exclusive complex with hVps15. GST-MTMR2, 60 ng, immobilized on glutathione-Sepharose beads was incubated with identical aliquots of V5-hVps15–containing cell lysates. After washing, increasing concentrations of Rab7-containing cell lysates (0, 1×, 10×) were added for incubation. Western blot shows coprecipitated proteins on beads and proteins in the supernatant (right panel). Binding of MTMR2 or Rab7 to hVps15 is competitive. (D) BHK cells overexpressing full-length V5-hVps15 (wt) or domain deletion mutants (Δ) (indicated in top panel) and Flag-MTMR2 were processed for IP with an anti-Flag mAb. Western blot shows coprecipitated hVps15 (left panel) and WCL (middle panel). Right graph shows the ratio of coprecipitated hVps15 to MTMR2 in each sample quantified with chemiluminescent signal on immunoblots by densitometry (mean ± SEM, n = 4; unpaired *t* test, two-tailed *p $<$ 0.05, **p $<$ 0.01). hVps15 WD40Δ exhibits diminished complex formation with MTMR2. (E) Equimolar amounts of GST-MTMR2 immobilized on glutathione-Sepharose beads were incubated with in vitro–synthesized, ^{35}S-L-methionine–labeled, full-length, hVps15 domain deletion mutants or individual hVps15 domains. Binding of the hVps15 proteins to GST-MTMR2 was quantified by phosphoimage analysis and binding was normalized relative to binding to GST (nonspecific binding equal to 1), which served as the negative control (mean ± SEM, n = 2, unpaired *t* test, two-tailed *p $<$ 0.05). hVps15 WD40Δ exhibits diminished complex formation with MTMR2, but binding is reconstituted with a HEAT/WD40 domain. Representative binding data are shown in Supplementary Figure S6 online. (F) BHK cells overexpressing Flag-MTMR2wt or Flag-MTMR2 coli domain deletion mutant (CoilΔ) (indicated in top panel) with V5-hVps15 were processed for IP with an anti-Flag mAb. Western blot shows coprecipitated hVps15 (bottom panel). The MTMR2 coil domain is dispensable for binding to hVps15. (G) Equimolar amounts of full-length GST-MTMR2, GST-PH, GST-PTP, GST-Coil, or GST proteins were purified and confirmed with Coomassie staining (top panel). The GST fusion proteins immobilized on glutathione-Sepharose beads were incubated with equal amount V5-hVps15–containing cell lysates. Western blot shows coprecipitated hVps15 (bottom panel). Both the PH and PTP domains of MTMR2 bind to hVps15 independently.

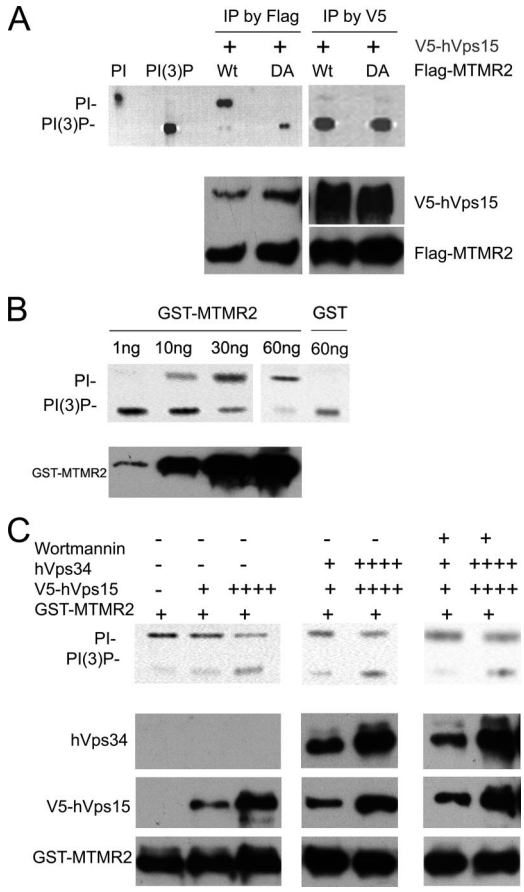

Figure 7. Binding of hVps15 inhibits MTMR2 PI(3)P phosphatase activity. (A) BHK cells overexpressing Flag-MTMR2wt or Flag-MTMR2D320A (catalytically inactive mutant) and V5-hVps15 were processed for immunoprecipitation (IP) with anti-Flag and anti-V5 antibodies, respectively. Western blot shows MTMR2 or hVps15 in the precipitated complex (bottom panel). The precipitated hVps15/MTMR2 complex was monitored for PI(3)P phosphatase activity with NBD6-PI(3)P substrate. Reaction products together with NBD6-PI and NBD6-PI(3)P standards were resolved by TLC with migration as indicated (top panel). The hVps15/MTMR2 complex IP by hVps15 lacks phosphatase activity. (B) The minimum amount of GST-MTMR2 required to convert 1.5 μg NBD6-PI(3)P into NBD6-PI within 15 min in the phosphatase assay was titrated to be 60 ng. GST, 60 ng, served as controls (top panel). Western blot shows the titrated GST-MTMR2 in the assay (bottom panel). (C) GST-MTMR2 (60 ng) immobilized on glutathione-Sepharose beads was incubated with increasing concentrations of V5-hVps15-containing or hVps34/V5-hVps15–containing cell lysates. Wortmannin was added in indicated samples. Phosphatase reaction products were resolved by TLC with the migration of PI and PI(3)P as indicated (top panel). Western blot shows the amounts of each protein in the phosphatase assay (bottom panel). Binding of hVps15 inactivates MTMR2 in a dose-dependent manner. The presence of the hVps34 does not shift the equilibrium in favor of PI(3)P production nor does the presence of wortmannin increase the production of PI.

hVps34wt did not shift the equilibrium in favor of PI(3)P production (Figure 7C) nor did the presence of the hVps34 kinase dead mutant increase the production of PI (data not shown) as would be expected if PI 3-kinase activity were playing a role in reconverting the product of MTMR2 activity back to PI(3)P. The addition of the PI 3-kinase inhibitor wortmannin also did not change the results (Figure 7C). On the basis of the cumulative data, we conclude that hVps15 binding inhibits MTMR2 PI(3)P phosphatase activity by interfering with substrate binding and/or blocking the enzyme active site (Figure 6G).

DISCUSSION

MTM1 and MTMR2 Act Sequentially on the Endocytic Pathway

Neuromuscular disorders are in some cases attributed to mutations in genes whose products have known functions in endocytic membrane trafficking. For example, mutations in dynamin 2, which controls internalization from the plasma membrane, were reported in dominant cases of centronuclear myopathy (Bitoun *et al.*, 2005). Mutations in Rab7, which controls transport to late endosomes, result in axonal dysfunction and sensory neuropathy classified as Charcot-Marie-Tooth disease type 2B (CMT2B; Niemann *et al.*, 2006; Spinosa *et al.*, 2008). Yet the functions in membrane trafficking of the MTM1 and MTMR2 lipid phosphatases, which are known to result in neuromuscular diseases, has not been clearly defined due to conflicting published reports on their cellular activities (Laporte *et al.*, 1996; Bolino *et al.*, 2000; Kim *et al.*, 2002; Chaussade *et al.*, 2003; Tsujita *et al.*, 2004; Lorenzo *et al.*, 2006). Earlier reports differentially ascribed MTM1 function to early or late endosomes, and there were conflicting reports regarding endosomal function of MTMR2 (Kim *et al.*, 2002; Chaussade *et al.*, 2003; Tsujita *et al.*, 2004; Lorenzo *et al.*, 2006). Several considerations suggest all data are consistent with MTM1 function on early endosomes. In agreement with others, we found overexpression of MTM1 causes the loss of EEA1 membrane association, which serves as a sensitive measure of early endosomal PI(3)P depletion (Chaussade *et al.*, 2003; Cao *et al.*, 2007). The late endosomal function of MTM1 was based on colocalization with the PIKfyve PI(3,5)P_2 kinase and inhibition of EGFR degradation (Tsujita *et al.*, 2004). However, PIKfyve has recently been shown to be important for early endosome dynamics (Ikonomov *et al.*, 2006), and previous EGFR degradation time course had insufficient resolution to distinguish early versus late endocytic events, suggesting that our data are not in conflict with the earlier report (Tsujita *et al.*, 2004). In two reports where MTMR2 was overexpressed, differential effects on PI(3)P were reported and there was lack of consensus as to any endosomal function (Kim *et al.*, 2002; Lorenzo *et al.*, 2006). As we show here, overexpressed MTMR2, has no impact on EEA1 membrane association, but does alter late endosomal PI(3)P levels and affects late EGFR trafficking steps. Our careful combination of multiple biochemical and morphological assays has clarified conflicting results in the literature and provides the first direct evidence that MTMR2, like MTM1 functions on the endocytic pathway.

Previous studies suggested myotubularins may or may not function by mass action (Kim *et al.*, 2002; Lorenzo *et al.*, 2006), but we show definitively that they regulate distinct subcellular pools of PI(3)P and PI(3,5)P_2 through their specific membrane recruitment to early and/or late endosomes. Though Kim considered that MTMR2 might utilize a different cellular pool of PI(3)P, experimental evidence was lacking possibly because of insensitivity of GST-2xFYVE^{Hrs} staining of fixed cells to visualize changes in PI(3)P (Kim *et al.*, 2002). Here, the local regulation of phosphoinositides by the myotubularins was shown to be important for the control of sequential steps in endocytic membrane trafficking.

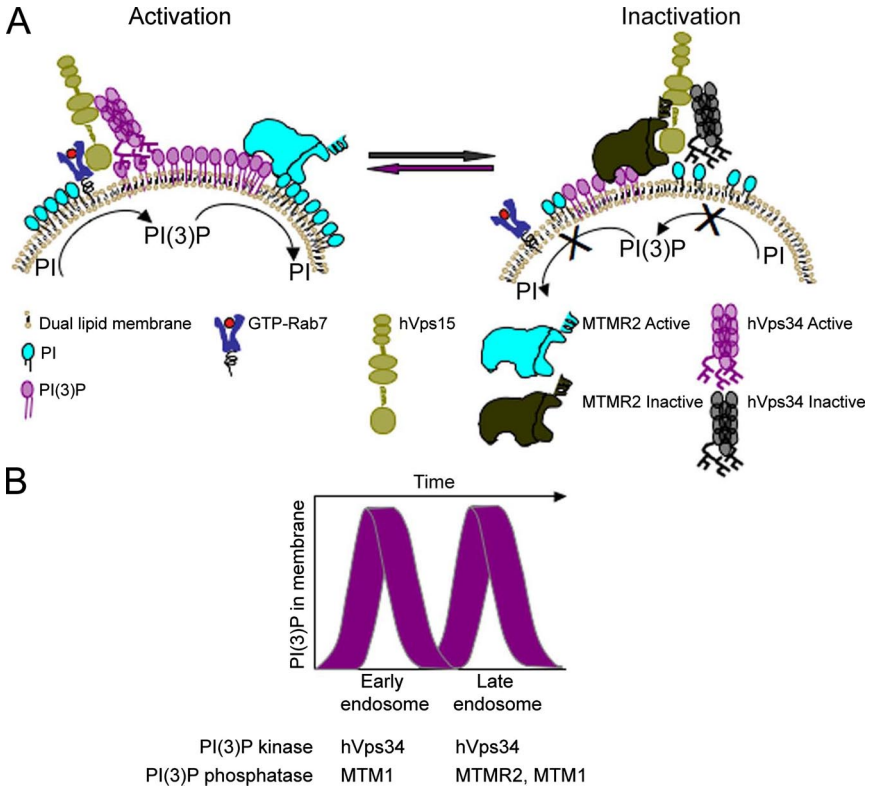

Figure 8. Model for coordinate regulation of PI(3)P homeostasis and endocytosis through the interplay between the hVps34/hVps15 lipid kinase complex and myotubularin phosphatases. (A) The hVps34/hVps15 lipid kinase complex is recruited or activated on endosomes by activated Rab GTPases and generates a localized burst of PI(3)P. Membrane recruitment of the myotubularins or their clustering in PI(3)P domains initiates PI(3)P degradation. Interaction of the myotubularin with the hVps34/hVps15 lipid kinase complex on endosomes simultaneously displaces the Rab GTPase required for hVps34/hVps15 activation and occludes the phosphatase domain, causing inactivation of the myotubularin. (B) Endosomes may undergo waves of PI(3)P synthesis and degradation in response to cycles of hVps34/hVps15 activation and inactivation. Such a mechanism allows the acute recruitment and release or activation and inactivation of trafficking machinery components for temporal regulation of membrane transport.

MTM1, which when mutant causes X-linked myotubular/centronuclear myopathy, was found to play a primary role in the egress of EGFR from early endosomes. MTMR2, which when mutant causes a severe demyelinating hereditary motor and sensory neuropathy (autosomal recessive CMT4B1), regulates the subsequent transit of EGFR out of late endosomes. Because growth factor receptor signaling is well known to be remodeled during transit on the endocytic pathway (Panopoulou *et al.*, 2002; Grimes and Miettinen, 2003; Miaczynska *et al.*, 2004; Teis *et al.*, 2006), the longevity and accumulation of internalized, activated receptors in different endosomal compartments offers the first functional explanation for the distinct disease etiologies resulting from mutant MTM1 or MTMR2. Our findings also support the integrated function of Rab7 and MTMR2 in PI(3)P mediated late endosomal sorting and trafficking events. Previous studies showed a correlation between disease phenotypes and cellular pathways in two very closely related forms of CMT disease. The MTMR13 gene product, which when mutant causes CMT4B2, was found to form a functional complex with MTMR2 (CMT4B1) that increased phosphatase activity (Azzedine *et al.*, 2003; Robinson and Dixon, 2005; Berger *et al.*, 2006). Although mutations in Rab7 or MTMR2 similarly result in axonal dysfunction, the fact that the two proteins do not interact directly may explain why mutations in Rab7 result in adult onset disease (CMT2B) and loss of MTMR2 phosphatase function results in the more severe, childhood onset, autosomal recessive disease CMT4B1 (Berger *et al.*, 2002; Verhoeven *et al.*, 2003; Houlden *et al.*, 2004; Meggouh *et al.*, 2006; Spinosa *et al.*, 2008). In sum, we have identified distinct and sequential functions of MTM1 and MTMR2 in endocytic trafficking and identified interconnected pathways involving MTMR2 and Rab7 on late endosomes that are logical in a disease related context.

Coordinate Endosomal PI(3)P Synthesis and Degradation Regulates Endosomal Transport

Spatiotemporal regulation of PI(3)P plays a pivotal role in receptor sorting on the endocytic pathway, as best exemplified by EGFR (Carpenter and Cohen, 1990). Depletion of endosomal PI(3)P established that PI(3)P is essential for intralumenal vesicle formation and endosomal sorting of EGFR (Futter *et al.*, 2001; Lu *et al.*, 2003; Petiot *et al.*, 2003; Tsujita *et al.*, 2004; Johnson *et al.*, 2006). Here we demonstrate that increasing endosomal PI(3)P levels 2–3-fold by siRNA-mediated gene silencing of PI 3-phosphatases also impairs endosomal EGFR sorting, suggesting there are optimal PI(3)P levels and too much or too little has negative consequences. The importance of overall PI(3)P balance suggests that endosomal PI(3)P synthesis and degradation must be tightly coordinated for proper growth factor receptor endocytosis and sorting.

The demonstration that MTMR2 interacts with the hVps34 PI 3-kinase lends new mechanistic insight as to how spatiotemporal regulation may be achieved (Figure 8, A and B). Active Rab5 or Rab7 at the membrane are thought to begin the cycle by binding and recruiting the hVps34/hVps15 PI 3-kinase complex to early or late endosomes, respectively (Stenmark *et al.*, 1994; Stein *et al.*, 2003). However, it is also conceivable that a pool of the hVps34/hVps15 PI 3-kinase complex may be resident on endosomal membranes in an inactive myotubularin-bound state and Rab activation initiates myotubularin displacement and kinase activation. On activation the PI 3-kinase complex generates a wave of local PI(3)P synthesis and serves as a recognition site for FYVE-domain proteins and the PH-GRAM-domain containing myotubularins. Membrane bound phosphatases begin the process of degrading the PI(3)P until they again become complexed with hVps34/hVps15 and displace the Rab5 or

Rab7 GTPase. MTMR2 phosphatase activity is inhibited when bound to the hVps34/hVps15 kinase complex most likely due to steric occlusion of the catalytic PTP-domain upon hVps15 binding. Alternatively, the PH-GRAM-domain, which is responsible for substrate and to some extent hVps15 binding, may limit substrate access when in the complex. Interestingly, the MTMR2 coiled-coil domain (important for binding to the inactive MTMR13, membrane recruitment and activation) was not involved in hVps15 interaction. Thus, future studies will be required to determine if MTMR13 is present together with MTMR2 in the lipid kinase complex and what influence this may have on MTMR2 activity. We suppose that lipid kinase activity is simultaneously diminished when hVps34/hVps15 are complexed to the phosphatase because MTMR2 binding precludes hVps15 interaction with Rab7, an interaction that is critical for hVps34 kinase activity. Thus, MTMR2 binding to hVps15 may simultaneously shut down both PI(3)P synthesis and degradation. Such a mechanism, provides tight temporal and spatial control over local PI(3)P levels and may account for the sequential waves of PI(3)P synthesis and degradation that have been reported to occur during phagosome maturation (Shin *et al.*, 2005; Yeung *et al.*, 2006). Similar cycles of protein activation and inactivation have been postulated to be important in Rab GTPase function (Rybin *et al.*, 1996).

In conclusion, the sequential regulation of PI(3)P by the myotubularins on early and late endosomes ensures timely receptor sorting and signal transduction, as well as spatiotemporal control over phosphoinositides. The demonstrated functions of MTM1 and MTMR2 in endosomal PI(3)P homeostasis and growth factor receptor down-regulation suggests that abnormalities in these processes may be key in the development of human myopathy and neuropathy.

ACKNOWLEDGMENTS

We gratefully acknowledge E. Romero for expert technical assistance, Dr. J. Dong for guidance during early project phases, Dr. R. Lee and G. Phillips for expert microscopy technical support, Dr. R. Glew for his writing class, Dr. K. Caldwell for helpful discussions and critically reading the manuscript, Dr. L. Weisman for GroP standards, and K. Bruner for advice and assistance in the application of the PI(3)P mass strip assay (Echelon Research Labs). Images in this article were generated in the UNM Cancer Center Fluorescence Microscopy Facility, supported as detailed on http://hsc.unm.edu/crtc/microscopy/Facility.html. DNA Research Services and the KUGR-UNM Genomics Resource provided invaluable assistance and instrumentation for DNA sequencing, Nanodrop quantification, and quantitative real-time PCR. This work was generously supported by National Science Foundation Grant MCB0446179 to A.W.N. Opinions, findings, and conclusions are those of the author(s) and not necessarily the views of the National Science Foundation. This work was also supported by grants from the American Diabetes Association and National Institute of Diabetes and Digestive and Kidney Diseases Grant DK070679 to J.M.B. and by INSERM, Centre National de la Recherche Scientifique, Collège de France, and grants from the Association Française contre les Myopathies to J.L.

REFERENCES

Azzedine, H. *et al.* (2003). Mutations in MTMR13, a new pseudophosphatase homologue of MTMR2 and Sbf1, in two families with an autosomal recessive demyelinating form of Charcot-Marie-Tooth disease associated with early-onset glaucoma. Am. J. Hum. Genet. *72*, 1141–1153.

Backer, J. M., Myers, M. J., Sun, X. J., Chin, D., Shoelson, S., Miralpeix, M., and White, M. (1993). Association of IRS-1 with the insulin receptor and the phosphatidylinositol 3′-kinase. Formation of binary and ternary signaling complexes in intact cells. J. Biol. Chem. *268*, 8204–8212.

Begley, M. J., and Dixon, J. (2005). The structure and regulation of myotubularin phosphatases. Curr. Opin. Struct. Biol. *15*, 614–620.

Berger, P., Berger, I., Schaffitzel, C., Tersar, K., Volkmer, B., and Suter, U. (2006). Multi-level regulation of myotubularin-related protein-2 phosphatase activity by myotubularin-related protein-13/set-binding factor-2. Hum. Mol. Genet. *15*, 569–579.

Berger, P., Bonneick, S., Willi, S., Wymann, M., and Suter, U. (2002). Loss of phosphatase activity in myotubularin-related protein 2 is associated with Charcot-Marie-Tooth disease type 4B1. Hum. Mol. Genet. *11*, 1569–1579.

Bitoun, M. *et al.* (2005). Mutations in dynamin 2 cause dominant centronuclear myopathy. Nat. Genet. *37*, 1207–1209.

Blondeau, F., Laporte, J., Bodin, S., Superti-Furga, G., Payrastre, B., and Mandel, J. (2000). Myotubularin, a phosphatase deficient in myotubular myopathy, acts on phosphatidylinositol 3-kinase and phosphatidylinositol 3-phosphate pathway. Hum. Mol. Genet. *9*, 2223–2229.

Bolino, A. *et al.* (2000). Charcot-Marie-Tooth type 4B is caused by mutations in the gene encoding myotubularin-related protein-2. Nat. Genet. *25*, 17–19.

Cao, C., Laporte, J., Backer, J., Wandinger-Ness, A., and Stein, M. (2007). Myotubularin lipid phosphatase binds the hVPS15/hVPS34 lipid kinase complex on endosomes. Traffic *8*, 1052–1067.

Carpenter, G., and Cohen, S. (1990). Epidermal growth factor. J. Biol. Chem. *265*, 7709–7712.

Chaussade, C. *et al.* (2003). Expression of myotubularin by an adenoviral vector demonstrates its function as a phosphatidylinositol 3-phosphate [PtdIns(3)P] phosphatase in muscle cell lines: involvement of PtdIns(3)P in insulin-stimulated glucose transport. Mol. Endocrinol. *17*, 2448–2460.

Christoforidis, S., Miaczynska, M., Ashman, K., Wilm, M., Zhao, L., Yip, S. C., Waterfield, M., Backer, J., and Zerial, M. (1999). Phosphatidylinositol-3-OH kinases are Rab5 effectors. Nat. Cell Biol. *1*, 249–252.

Dadabay, C., Patton, E., Cooper, J., and Pike, L. (1991). Lack of correlation between changes in polyphosphoinositide levels and actin/gelsolin complexes in A431 cells treated with epidermal growth factor. J. Cell Biol. *112*, 1151–1156.

Feng, Y., Press, B., Chen, W., Zimmerman, J., and Wandinger-Ness, A. (2001). Expression and properties of Rab7 in endosome function. Methods Enzymol. *329*, 175–187.

Futter, C., Collinson, L., Backer, J., and Hopkins, C. (2001). Human VPS34 is required for internal vesicle formation within multivesicular endosomes. J. Cell Biol. *155*, 1251–1264.

Gamou, S., Kim, Y. S., and Shimizu, N. (1984). Different responses to EGF in two human carcinoma cell lines, A431 and UCVA-1, possessing high numbers of EGF receptors. Mol. Cell Endocrinol. *37*, 205–213.

Gillooly, D., Morrow, I., Lindsay, M., Gould, R., Bryant, N., Gaullier, J., Parton, R., and Stenmark, H. (2000). Localization of phosphatidylinositol 3-phosphate in yeast and mammalian cells. EMBO J. *19*, 4577–4588.

Grimes, M., and Miettinen, H. (2003). Receptor tyrosine kinase and G-protein coupled receptor signaling and sorting within endosomes. J. Neurochem. *84*, 905–918.

Houlden, H., King, R., Muddle, J., Warner, T., Reilly, M., Orrell, R., and Ginsberg, L. (2004). A novel RAB7 mutation associated with ulcero-mutilating neuropathy. Ann. Neurol. *56*, 586–590.

Hudson, L., Toscano, W. J., and Greenlee, W. (1986). 2,3,7,8-Tetrachlorodibenzo-p-dioxin (TCDD) modulates epidermal growth factor (EGF) binding to basal cells from a human keratinocyte cell line. Toxicol. Appl. Pharmacol. *82*, 481–492.

Ikonomov, O., Sbrissa, D., Foti, M., Carpentier, J., and Shisheva, A. (2003). PIKfyve controls fluid phase endocytosis but not recycling/degradation of endocytosed receptors or sorting of procathepsin D by regulating multivesicular body morphogenesis. Mol. Biol. Cell *14*, 4581–4591.

Ikonomov, O., Sbrissa, D., and Shisheva, A. (2006). Localized PtdIns 3,5-P2 synthesis to regulate early endosome dynamics and fusion. Am. J. Physiol. Cell Physiol. *291*, C393–C404.

Johnson, E., Overmeyer, J., Gunning, W., and Maltese, W. (2006). Gene silencing reveals a specific function of hVps34 phosphatidylinositol 3-kinase in late versus early endosomes. J. Cell Sci. *119*, 1219–1232.

Kim, S. A., Taylor, G. S., Torgersen, K., and Dixon, J. (2002). Myotubularin and MTMR2, phosphatidylinositol 3-phosphatases mutated in myotubular myopathy and type 4B Charcot-Marie-Tooth disease. J. Biol. Chem. *277*, 4526–4531.

Krupp, M. N., Connolly, D., and Lane, M. (1982). Synthesis, turnover, and down-regulation of epidermal growth factor receptors in human A431 epidermoid carcinoma cells and skin fibroblasts. J. Biol. Chem. *257*, 11489–11496.

Laporte, J., Hu, L., Kretz, C., Mandel, J., Kioschis, P., Coy, J. F., Klauck, S., Poustka, A., and Dahl, N. (1996). A gene mutated in X-linked myotubular myopathy defines a new putative tyrosine phosphatase family conserved in yeast. Nat. Genet. *13*, 175–182.

Laporte, J., Liaubet, L., Blondeau, F., Tronchere, H., Mandel, J., and Payrastre, B. (2002). Functional redundancy in the myotubularin family. Biochem. Biophys. Res. Commun. *291*, 305–312.

Lorenzo, O., Urbe, S., and Clague, M. J. (2006). Systematic analysis of myotubularins: heteromeric interactions, subcellular localisation and endosome related functions. J. Cell Sci. *119*, 2953–2959.

Lu, Q., Hope, L., Brasch, M., Reinhard, C., and Cohen, S. (2003). TSG101 interaction with HRS mediates endosomal trafficking and receptor down-regulation. Proc. Natl. Acad. Sci. USA *100*, 7626–7631.

McCawley, L., O'brien, P., and Hudson, L. (1997). Overexpression of the epidermal growth factor receptor contributes to enhanced ligand-mediated motility in keratinocyte cell lines. Endocrinology *138*, 121–127.

Meggouh, F., Bienfait, H., Weterman, M., De Visser, M., and Baas, F. (2006). Charcot-Marie-Tooth disease due to a de novo mutation of the RAB7 gene. Neurology *67*, 1476–1478.

Miaczynska, M., Christoforidis, S., Giner, A., Shevchenko, A., Uttenweiler-Joseph, S., Habermann, B., Wilm, M., Parton, R., and Zerial, M. (2004). APPL proteins link Rab5 to nuclear signal transduction via an endosomal compartment. Cell *116*, 445–456.

Murray, J. T., Panaretou, C., Stenmark, H., Miaczynska, M., and Backer, J. (2002). Role of Rab5 in the recruitment of hVps34/p150 to the early endosome. Traffic *3*, 416–427.

Nicot, A., Fares, H., Payrastre, B., Chisholm, A., Labouesse, M., and Laporte, J. (2006). The phosphoinositide kinase PIKfyve/Fab1p regulates terminal lysosome maturation in *Caenorhabditis elegans*. Mol. Biol. Cell *17*, 3062–3074.

Niemann, A., Berger, P., and Suter, U. (2006). Pathomechanisms of mutant proteins in Charcot-Marie-Tooth disease. Neuromolecular Med. *8*, 217–242.

Panopoulou, E., Gillooly, D., Wrana, J., Zerial, M., Stenmark, H., Murphy, C., and Fotsis, T. (2002). Early endosomal regulation of Smad-dependent signaling in endothelial cells. J. Biol. Chem. *277*, 18046–18052.

Petiot, A., Faure, J., Stenmark, H., and Gruenberg, J. (2003). PI3P signaling regulates receptor sorting but not transport in the endosomal pathway. J. Cell Biol. *162*, 971–979.

Pettitt, T., Dove, S., Lubben, A., Calaminus, S., and Wakelam, M. (2006). Analysis of intact phosphoinositides in biological samples. J. Lipid Res. *47*, 1588–1596.

Robinson, F., and Dixon, J. (2005). The phosphoinositide-3-phosphatase MTMR2 associates with MTMR13, a membrane-associated pseudophosphatase also mutated in type 4B Charcot-Marie-Tooth disease. J. Biol. Chem. *280*, 31699–31707.

Rudge, S. A., Anderson, D., and Emr, S. D. (2004). Vacuole size control: regulation of PtdIns(3,5)P2 levels by the vacuole-associated Vac14-Fig4 complex, a PtdIns(3,5)P2-specific phosphatase. Mol. Biol. Cell *15*, 24–36.

Rybin, V., Ullrich, O., Rubino, M., Alexandrov, K., Simon, I., Seabra, M., Goody, R., and Zerial, M. (1996). GTPase activity of Rab5 acts as a timer for endocytic membrane fusion. Nature *383*, 266–269.

Sbrissa, D., Ikonomov, O., and Shisheva, A. (2002). Phosphatidylinositol 3-phosphate-interacting domains in PIKfyve. Binding specificity and role in PIKfyve. Endomembrane localization. J. Biol. Chem. *277*, 6073–6079.

Sbrissa, D., and Shisheva, A. (2005). Acquisition of unprecedented phosphatidylinositol 3,5-bisphosphate rise in hyperosmotically stressed 3T3–L1 adipocytes, mediated by ArPIKfyve-PIKfyve pathway. J. Biol. Chem. *280*, 7883–7889.

Shin, H. *et al.* (2005). An enzymatic cascade of Rab5 effectors regulates phosphoinositide turnover in the endocytic pathway. J. Cell Biol. *170*, 607–618.

Shisheva, A. (2008). PIKfyve: partners, significance, debates and paradoxes. Cell Biol. Int. *32*, 591–604.

Simonsen, A., Wurmser, A., Emr, S. D., and Stenmark, H. (2001). The role of phosphoinositides in membrane transport. Curr. Opin. Cell Biol. *13*, 485–492.

Spinosa, M. R., Progida, C., De Luca, A., Colucci, A., Alifano, P., and Bucci, C. (2008). Functional characterization of Rab7 mutant proteins associated with Charcot-Marie-Tooth type 2B disease. J. Neurosci. *28*, 1640–1648.

Stein, M., Cao, C., Tessema, M., Feng, Y., Romero, E., Welford, A., and Wandinger-Ness, A. (2005). Interaction and functional analyses of human VPS34/p150 phosphatidylinositol 3-kinase complex with Rab7. Methods Enzymol. *403*, 628–649.

Stein, M., Feng, Y., Cooper, K., Welford, A., and Wandinger-Ness, A. (2003). Human VPS34 and p150 are Rab7 interacting partners. Traffic *4*, 754–771.

Stenmark, H., Parton, R., Steele-Mortimer, O., Lutcke, A., Gruenberg, J., and Zerial, M. (1994). Inhibition of rab5 GTPase activity stimulates membrane fusion in endocytosis. EMBO J. *13*, 1287–1296.

Stephens, L., Hawkins, P., and Downes, C. (1989). Metabolic and structural evidence for the existence of a third species of polyphosphoinositide in cells: D-phosphatidyl-myo-inositol 3-phosphate. Biochem. J. *259*, 267–276.

Taylor, G., and Dixon, J. (2001). An assay for phosphoinositide phosphatases utilizing fluorescent substrates. Anal. Biochem. *295*, 122–126.

Taylor, G., Maehama, T., and Dixon, J. (2000). Inaugural article: myotubularin, a protein tyrosine phosphatase mutated in myotubular myopathy, dephosphorylates the lipid second messenger, phosphatidylinositol 3-phosphate. Proc. Natl. Acad. Sci. USA *97*, 8910–8915.

Teis, D. *et al.* (2006). p14-MP1-MEK1 signaling regulates endosomal traffic and cellular proliferation during tissue homeostasis. J. Cell Biol. *175*, 861–868.

Tronchere, H., Laporte, J., Pendaries, C., Chaussade, C., Liaubet, L., Pirola, L., Mandel, J., and Payrastre, B. (2004). Production of phosphatidylinositol 5-phosphate by the phosphoinositide 3-phosphatase myotubularin in mammalian cells. J. Biol. Chem. *279*, 7304–7312.

Tsujita, K., Itoh, T., Ijuin, T., Yamamoto, A., Shisheva, A., Laporte, J., and Takenawa, T. (2004). Myotubularin regulates the function of the late endosome through the gram domain-phosphatidylinositol 3,5-bisphosphate interaction. J. Biol. Chem. *279*, 13817–13824.

Verhoeven, K. *et al.* (2003). Mutations in the small GTP-ase late endosomal protein RAB7 cause Charcot-Marie-Tooth type 2B neuropathy. Am. J. Hum. Genet. *72*, 722–727.

Walsh, J., Caldwell, K., and Majerus, P. (1991). Formation of phosphatidylinositol 3-phosphate by isomerization from phosphatidylinositol 4-phosphate. Proc. Natl. Acad. Sci. USA *88*, 9184–9187.

Wymann, M., Bulgarelli-Leva, G., Zvelebil, M., Pirola, L., Vanhaesebroeck, B., Waterfield, M., and Panayotou, G. (1996). Wortmannin inactivates phosphoinositide 3-kinase by covalent modification of Lys-802, a residue involved in the phosphate transfer reaction. Mol. Cell Biol. *16*, 1722–1733.

Yeung, T., Ozdamar, B., Paroutis, P., and Grinstein, S. (2006). Lipid metabolism and dynamics during phagocytosis. Curr. Opin. Cell Biol. *18*, 429–437.